20th AIAA Computational Fluid Dynamics Conference
27 - 30 June 2011, Honolulu, Hawaii

AIAA 2011-3855

The Role of Dual Consistency in Functional Accuracy: Error Estimation and Superconvergence

Jason E. Hicken* and David W. Zingg †

Institute for Aerospace Studies, University of Toronto, Toronto, Ontario, M3H 5T6, Canada

A discretization is dual consistent if it leads to a discrete dual problem that is a consistent approximation of the corresponding continuous dual problem. This paper investigates the impact of dual consistency on high-order summation-by-parts finite-difference schemes. In particular, dual consistent schemes lead to superconvergent functionals and accurate functional error estimates. Numerical examples demonstrate that dual consistent schemes significantly outperform dual inconsistent schemes in terms of functional accuracy and error-estimate effectiveness. The influence of dual consistency on general discretizations is discussed.

I. Introduction

In many engineering applications, computational fluid dynamics is used to estimate the value of a functional that depends on flow quantities. The lift and drag forces are two common examples. In this context, we consider an algorithm efficient if it computes the functional more accurately than a baseline algorithm using the same computational resources and time.

One way to increase the accuracy and, potentially, the efficiency of a functional estimate is to increase the accuracy of the solution itself. This is often a motivation for high-order discretization schemes. However, experience suggests that a discrete solution with a verified order of accuracy — including second-order — can produce functional estimates with erratic convergence behaviour and significantly delayed asymptotic convergence. For example, Vassberg and Jameson[1] considered subsonic and transonic flow around a modified NACA0012 airfoil. They demonstrated that several well-established solvers require a significant number of nodes ($> 2.5 \times 10^5$ in 2D) to reach the asymptotic-convergence regime and often exhibit sub-optimal convergence rates, even for subsonic flows.

The convergence behaviour of functional estimates was also studied recently by Salas and Atkins.[2] They showed that the error due to the quadrature rule can interact with the solution error, producing singularities in the functional convergence. A similar issue arises due to higher-order contributions to the solution error, i.e. when the solution itself is not yet in the region of asymptotic convergence. Indeed, their theoretical model of convergence bears a striking resemblance to several convergence results presented in Ref. 1.

In this paper we show that functional accuracy and convergence behaviour is strongly influenced by the (tacit) discretization of the adjoint equations. Adjoint, or dual, problems play an increasingly important role in computational fluid dynamics. Applications that use adjoint variables include optimization,[3–9] error control and estimation,[10–12] and mesh adaptation.[13–15]

Typically, the equations that govern the adjoint variables are derived in one of two ways. The continuous-adjoint approach, associated with Jameson's pioneering work in aerodynamic shape optimization,[4] derives the continuous adjoint equations first, and then discretizes the primal and dual problems independently. In contrast, the discrete-adjoint approach[16,17] uses the discretized primal equations and functional to derive the linear system for the adjoint variables.

The two approaches have their advantages and disadvantages. The discrete adjoint equations are typically easier to derive, since they amount to an exercise in differentiation; thus, developers can use automatic

*Postdoctoral Fellow, AIAA Member, jehicken@stanford.edu

†Professor and Director, Canada Research Chair in Computational Aerodynamics, J. Armand Bombardier Foundation Chair in Aerospace Flight, Associate Fellow AIAA

differentiation[18] or the complex-step method[19,20] to populate the (transposed) Jacobian. In addition, discrete functional gradients based on the discrete adjoint variables can be made accurate to machine precision; consequently, advanced gradient-based optimization algorithms can be used for design problems.

The continuous-adjoint approach leads to a discretized system that is a consistent approximation to the dual problem, which has subtle but important consequences. For example, Collis and Heinkenschloss[21] found that the continuous-adjoint approach lead to control (design) variables with better asymptotic convergence properties when high-order elements were used in a SUPG finite-element discretization. Moreover, in functional error estimation, the adjoint solution is often interpolated onto a finer grid. Discrete-adjoint variables can be non-smooth and oscillatory, making this interpolation process difficult, if not invalid. The continuous adjoint variables are typically well behaved and straightforward to interpolate, because they converge to the infinite-dimensional solution.

Rather than choose between the discrete or continuous approaches, the approach advocated here is to discretize the primal equations such that the discrete adjoint equations are consistent with the dual problem. Such adjoint variables will lead to exact gradients, since they correspond with a discrete adjoint approach. In addition, because they also converge to the exact adjoint variables, they lead to some surprising behaviour from the functional, such as smooth convergence and even superconvergence.

The discretization strategy discussed above is called adjoint, or dual[a], consistency, and it is well-known in the finite-element community (see, e.g., Refs. 11, 22, 23). In this paper, we show that dual consistency is an important and desirable property beyond finite-element discretizations. In particular, we demonstrate that dual consistency can significantly impact the accuracy of functionals and error estimates for high-order summation-by-parts (SBP) finite-difference discretizations. The results suggest that dual consistency offers a potential solution to the type of irregular functional convergence discussed by Salas and Atkins[2]

We begin with an introduction to duality in Section II, where we also review the concept of dual consistency. In Section III we investigate the consequences of dual consistency for SBP finite-difference discretizations, namely superconvergent discrete functionals and improved functional error estimates. We verify the theory using several numerical experiments, which demonstrate the importance of dual consistency; these results are presented in Section IV. Finally, we conclude in Section V with a summary of the results and some conjectures regarding the importance of dual consistency for general discretizations.

II. Duality

This section presents a review of adjoint equations, duality, and dual consistency. We begin by introducing our notation.

Capital letters with a script type denote functions on a specified domain Ω. For example, $\mathcal{U}(x) \in C^p[0,1]$ is a function in the set of p-times differentiable functions that are square integrable on the interval $[0,1]$. Small roman letters in a serif type are used to indicate a function restricted to the grid, for example

$$u = \begin{bmatrix} \mathcal{U}(x_0) & \mathcal{U}(x_1) & \cdots & \mathcal{U}(x_n) \end{bmatrix}^T.$$

If a subscript h appears on a vector, for example, $u_h \in \mathbb{R}^{n+1}$, this indicates that the vector is the solution of a difference equation on a mesh with a nominal spacing h.

The "big-O" order notation is used to indicate various bounds. We write $F(h) = \mathrm{O}(h^p)$ if and only if $\exists\, M > 0$ and $h_\star > 0$ such that

$$|F(h)| \leq M h^p, \qquad \forall\, h < h_\star.$$

A. The Continuous Dual Problem

We review the concept of dual, or adjoint, consistency assuming a linear problem to avoid complications introduced by nonlinearity. See Ref. 11 for a discussion of how to handle nonlinear PDEs and functionals.

Let L be a linear differential operator and consider the scalar boundary-value problem (BVP)

$$L\mathcal{U} - \mathcal{F} = 0, \qquad \forall\, x \in \Omega, \tag{1}$$

where $\mathcal{F} \in L^2(\Omega)$ is a spatially varying function independent of $\mathcal{U}$. For simplicity, we assume that (1) is subject to appropriate homogeneous boundary conditions that produce a well-posed problem; for more general boundary conditions see Ref. 24.

[a] dual and adjoint will be used interchangeably throughout this paper

Given that the PDE (1) is well posed, we can consider a linear functional of the solution $\mathcal{U}$:

$$\mathcal{J}(\mathcal{U}) = (\mathcal{G},\mathcal{U})_\Omega, \tag{2}$$

where $(,)_\Omega$ denotes an integral inner product on Ω and $\mathcal{G} \in L^2(\Omega)$. In general, $\mathcal{J}$ will also include boundary terms. Taking the inner product of the PDE with the generic function $\mathcal{V} \in L^2(\Omega)$, the functional can be written as

$$\begin{aligned}\mathcal{J}(\mathcal{U}) &= (\mathcal{G},\mathcal{U})_\Omega - (\mathcal{V}, L\mathcal{U} - \mathcal{F})_\Omega, \\ &= (\mathcal{V},\mathcal{F})_\Omega - (L^*\mathcal{V} - \mathcal{G},\mathcal{U})_\Omega - \mathcal{B}_{\partial\Omega}(\mathcal{U},\mathcal{V})\end{aligned} \tag{3}$$

where the formal adjoint operator L^* is defined by the extended Green's identity:[24]

$$\mathcal{B}_{\partial\Omega}(\mathcal{U},\mathcal{V}) = (\mathcal{V}, L\mathcal{U})_\Omega - (L^*\mathcal{V},\mathcal{U})_\Omega, \tag{4}$$

where $\mathcal{B}_{\partial\Omega}$ denotes an operator defined on the boundary of Ω that is bilinear in $\mathcal{U}$, $\mathcal{V}$, and their derivatives.

Presently, we have placed no conditions on $\mathcal{V}$, so (3) is a nonunique expression for the functional $\mathcal{J}$. The dual problem corresponds with the particular choice where we demand (3) be independent of $\mathcal{U}$ (more precisely, independent of variations $\delta\mathcal{U}$ in $\mathcal{U}$). Then we must have

$$\begin{aligned} L^*\,\mathcal{V} - \mathcal{G} &= 0, \qquad \forall\, x \in \Omega, \\ \mathcal{B}_{\partial\Omega}(\mathcal{U},\mathcal{V}) &= 0, \qquad \forall\, x \in \partial\Omega. \end{aligned} \tag{5}$$

The boundary conditions on $\mathcal{V}$ are the minimal set of conditions necessary to make $\mathcal{B}_{\partial\Omega}$ vanish, taking the boundary conditions on $\mathcal{U}$ into account.

If we assume the dual BVP (5) is well posed, with solution $\mathcal{V}$, then the second and third terms in (3) vanish, and the functional becomes

$$\mathcal{J}(\mathcal{U}) = \mathcal{J}(\mathcal{V}) = (\mathcal{V},\mathcal{F})_\Omega.$$

Note that the roles of $\mathcal{F}$ and $\mathcal{G}$ in the primal formulation (i.e., the PDE (1) and $\mathcal{J}(\mathcal{U})$) are reversed in the adjoint formulation (i.e., the PDE (5) and $\mathcal{J}(\mathcal{V})$).

We illustrate the derivation of the dual problem on some concrete examples in the Appendix. For a more thorough introduction to the adjoint variables, see Ref. 25.

B. The Discrete Adjoint and Dual Consistency

For simplicity, we will confine our analysis to discretizations defined on a computational grid consisting of $n+1$ uniformly spaced points $x_k = kh$, $k = 0, 1, \ldots, n$, with mesh spacing $h = 1/n$. This implies the computational domain is the interval $[0, 1]$; if this is not the case, it is assumed that an invertible and sufficiently differentiable transformation can be introduced to map the domain to $[0, 1]$.

As discussed in the introduction, the concept of a dual problem has a discrete analog. Let

$$L_h u_h - f = 0 \tag{6}$$

be a discretization of (1), and let

$$J_h(u_h) = (g, u_h)_h$$

be a discrete approximation of the functional $\mathcal{J}$. In general, the linear operator $L_h : \mathbb{R}^{n+1} \to \mathbb{R}^{n+1}$ incorporates both the discretization of the PDE and the boundary conditions. Similarly, the discrete inner product $(,)_h : \mathbb{R}^{n+1} \times \mathbb{R}^{n+1} \to \mathbb{R}$ may include internal and boundary terms. Taking the discrete inner product of (6) with an arbitrary $v_h \in \mathbb{R}^{n+1}$, we have

$$\begin{aligned} J_h(u_h) &= (g, u_h)_h - (v_h, L_h u_h - f)_h \\ &= (v_h, f)_h - (L_h^* v_h - g, u_h)_h, \end{aligned}$$

where $(v_h, L_h u_h)_h = (L_h^* v_h, u_h)_h$ defines the discrete adjoint operator L_h^*. In analogy with (5), we define the discrete dual equation

$$L_h^* v_h - g = 0. \tag{7}$$

What is the relationship between the discrete system (7) and the continuous Adjoint PDE (5)? Moreover, what is the relationship between v_h and $\mathcal{V}$?

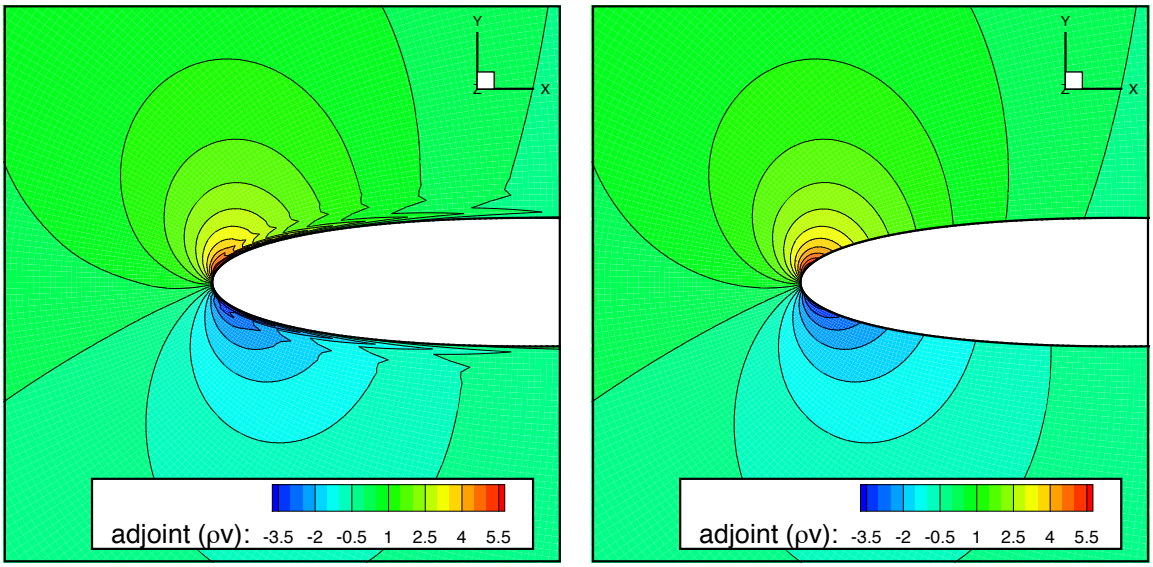

(a) dual inconsistent (b) dual consistent

Figure 1. Contours of the second component of the drag adjoint near the leading edge of the NACA0012 airfoil in a subsonic flow.

Definition (Dual (Adjoint) Consistency)**.** *A discrete operator L_h and functional J_h are dual (adjoint) consistent of order $q \geq 1$ with respect to a corresponding continuous PDE and functional if*

$$L_h^* v - g = O(h^q),$$

where v is the solution to the continuous dual problem projected onto the discrete solution space.

In other words, a discretization is dual consistent if it leads to a discrete dual problem that is a consistent discretization of the continuous dual PDE. This concept of dual consistency was first introduced by Lu in the context of discontinuous Galerkin discretizations.[22] It is important to recognize that dual consistency does not follow from consistency of the primal PDE discretization, in general.

Figure 1 illustrates the difference between a discrete adjoint field that is dual consistent and one that is dual inconsistent. The flow corresponds to a NACA0012 airfoil at Mach 0.5 and an angle of attack of 1.25 degrees; see Section IV.B.2 for additional details. The contours plotted are for the second component of the drag-adjoint vector. Significant oscillations are visible near the surface of the airfoil in the dual inconsistent results. In contrast, the dual consistent solution is smooth. We emphasize that the primal flow solution of both schemes does not exhibit any oscillations. As we shall see, the consequences of dual consistency are more than aesthetic.

Even if a discretization is dual consistent, it is not obvious that the discrete adjoint variables will converge to the continuous adjoint variables. For convergence, we also require stability of the discrete adjoint system (7). Fortunately, in many cases it is possible to infer the stability of the adjoint problem from the stability of the primal problem.

III. Dual Consistency and Summation-by-Parts Finite-Difference Discretizations

This section presents theoretical results regarding the impact of dual consistency on summation-by-parts (SBP) finite-difference discretizations. SBP finite-difference operators were developed by Kreiss and Scherer[26] to mimic the stability properties of Galerkin finite-element methods. The general class of SBP operators satisfies the following definition.

Definition (Summation-By-Parts Operator)**.** *The matrix $D \in \mathbb{R}^{(n+1)\times(n+1)}$ is a summation-by-parts oper-*

ator for the first derivative if it has the form

$$D = H^{-1}Q,$$

where $H \in \mathbb{R}^{(n+1)\times(n+1)}$ *is a symmetric-positive-definite weight matrix with entries* $H_{ij} = O(h)$*, and* $Q \in \mathbb{R}^{(n+1)\times(n+1)}$ *satisfies*

$$Q + Q^T = \text{diag}\,(-1, 0, 0, \ldots, 0, 1).$$

Furthermore, D *is a* $2s$*-order-accurate approximation to* d/dx *at the interior nodes,* $\{x_k\}_{k=r}^{n-r}$*, and a* τ*-order-accurate approximation at the boundary nodes,* $\{x_k\}_{k=0}^{r-1}$ *and* $\{x_k\}_{k=n-r+1}^{n}$*.*

In other words, an SBP operator is a first-derivative approximation that is "nearly" skew-symmetric with respect to the weight matrix H. An SBP operator has r boundary points at each end of the domain whose truncation error is order h^τ, and the remaining interior points have order h^{2s} truncation errors. The even order of accuracy for the internal nodes is a consequence of using centered-difference schemes consisting of s points on either side of the node in question, which provides the lowest error for a given stencil size.

We are primarily interested in SBP operators that have diagonal weight matrices H. Svärd[27] showed that such "diagonal-norm" SBP operators are necessary to guarantee time stability when coordinate transformations are used. Unfortunately, to achieve both stability and high-order accuracy, diagonal-norm SBP operators have interior stencils that are twice the accuracy of their boundary stencils (i.e., $\tau = s$). For example, a sixth-order interior scheme must be paired with a third-order boundary scheme, and this limits the global accuracy of the solution to fourth-order. The price paid for time stability is a decrease in solution accuracy for a given interior stencil size.

Despite a reduced solution accuracy relative to the interior stencil, diagonal-norm SBP operators can be used to construct dual consistent discretizations, which has important consequences for the accuracy of functional estimates.

A. Superconvergence of SBP-SAT Functional Estimates

For simplicity, we consider a scalar one-dimensional BVP; however, the results below have been shown to hold for elliptic equations and curvilinear multi-block grids,[28] and numerical experiments suggest that the results extend to nonlinear hyperbolic systems (see, for example, the results presented in Section IV).

Consider the BVP

$$\begin{aligned} \frac{\partial}{\partial x}(\lambda \mathcal{U}) &= \mathcal{F}, \qquad \forall\, x \in \Omega = [0,1], \\ \mathcal{U}(0) &= \mathcal{U}_L, \end{aligned} \tag{8}$$

where $\lambda(x) > 0$ is the spatially varying wave speed. A dual-consistent SBP discretization of this problem is given by

$$D\,(\Lambda u_h) = f - H^{-1} e_0 \lambda_0 \left(e_0^T u_h - \mathcal{U}_L\right) \tag{9}$$

where $e_0 = [1\ 0\ 0\ \cdots\ 0]^T$ and

$$\begin{aligned} \lambda_i &= \lambda(x_i), \qquad i = 0, \ldots, n, \\ \Lambda &= \text{diag}\,(\lambda_0, \lambda_1, \ldots, \lambda_N), \\ f &= \begin{bmatrix} \mathcal{F}(x_0) & \mathcal{F}(x_1) & \cdots & \mathcal{F}(x_n) \end{bmatrix}^T. \end{aligned}$$

In the above discretization, the boundary conditions are imposed weakly using simultaneous approximation terms[29,30] (SATs). There is some flexibility in the choice of SAT from a stability perspective, since we could multiply the penalty term by a scaling factor; however, the above choice of SAT ensures that the scheme is dual-consistent with respect to the discrete functional defined later.

The vector $u_h \in \mathbb{R}^{n+1}$ denotes the unique solution to the linear system (9). For diagonal-norm SBP operators with an s-order-accurate boundary closure, Gustafsson's theory[31] and numerical experiments suggest that the solution error $\|u_h - u\|_\infty$ is $\mathrm{O}(h^{s+1})$. Despite this bound on the accuracy of the discrete solution, the following theorem concludes that a discrete functional based on u_h can approximate the exact functional to order $2s$.

Theorem. *Let $\mathcal{J} : L^2[0,1] \to \mathbb{R}$ be a linear functional defined by*

$$\mathcal{J}(\mathcal{U}) = \int_0^1 \mathcal{G}\,\mathcal{U}\,dx + \alpha\,(\lambda\mathcal{U})|_{x=1}\,, \tag{10}$$

where $\mathcal{G} \in C^{2s}[0,1]$, and let $H^{-1}A \equiv H^{-1}(Q + e_0\,e_0^T)\Lambda$ denote the matrix appearing in the linear system (9). Assume the problem (8) is well posed and admits the solution $\mathcal{U} \in C^{2s}[0,1]$. Furthermore, assume the linear system (9) is nonsingular with solution $u_h \in \mathbb{R}^{n+1}$, and $\|A^{-T}H\|_\infty \leq C$ for some constant $C \in \mathbb{R}$, independent of n. Then the functional estimate

$$J_h(u_h) = (g, u_h)_H + \alpha\lambda_n(e_n^T u_h), \tag{11}$$

where

$$g = \begin{bmatrix}\mathcal{G}(x_0) & \mathcal{G}(x_1) & \cdots & \mathcal{G}(x_n)\end{bmatrix}^T,$$

is a $2s$-order-accurate approximation to $\mathcal{J}(\mathcal{U})$.

See Ref. 28 for the proof. Although not obvious from the statement of the theorem, the proof relies on the dual consistency of the SBP-SAT discretization. That is, the SBP-SAT discretization of a PDE and functional leads to a discrete dual problem that is a consistent, and sufficiently accurate, discretization of the dual PDE. If the difference operator did not satisfy the SBP property, or if there was a mismatch between the SAT penalties and the discrete functional definition, the functional estimate would not be superconvergent.

Thus, dual consistent SBP-SAT discretizations lead to superconvergent functional estimates, a result usually associated only with finite-element methods. However, we note that there are close connections between the discontinuous Galerkin FEM and SBP-SAT discretizations. For example, SBP discretizations can be formulated as a discrete variational statement, as the next section demonstrates.

B. Adjoint-Based Functional Error Estimation

The adjoint-weighted residual method has proven to be highly effective for both functional error estimation and output-based mesh adaptation.[32] Here we describe the extension of this method to SBP finite-difference discretizations for error estimation and highlight the role of dual consistency.

In order to define the adjoint-weighted residual method for SBP discretizations, we need to introduce a discrete representation of the residual. Consider the variational form of the BVP (8): find $\mathcal{U} \in \mathsf{W}$ such that

$$\begin{aligned}\mathcal{R}(\mathcal{U},\mathcal{V}) &= \int_\Omega \mathcal{V}\left(\frac{\partial}{\partial x}\,(\lambda\mathcal{U}) - \mathcal{F}\right)dx + \lambda\mathcal{V}(\mathcal{U} - \mathcal{U}_L)|_{x=0} \\ &= 0,\end{aligned} \tag{12}$$

$\forall\,\mathcal{V} \in \mathsf{Z}$, where W and Z are appropriate function spaces. The residual $\mathcal{R}$ can be approximated to order h^{2p} using the SBP operator D_p, where the subscript p denotes the accuracy of the boundary stencil:[33]

$$\begin{aligned}\mathcal{R}(\mathcal{U},\mathcal{V}) &= v^T H_p\left[D_p\,(\Lambda u_h) - f + H_p^{-1}e_0\,e_0^T\Lambda\,(u_h - \mathcal{U}_L e_0)\right] + \mathrm{O}(h^{2p}) \\ &= R_{h,p}(u,v) + \mathrm{O}(h^{2p}).\end{aligned} \tag{13}$$

We can now state the bounds on the accuracy of the adjoint-weighted-residual error estimate.

Theorem. *For a given mesh size n, let D_p and D_q denote diagonal-norm SBP operators with boundary stencils of p- and q-order accuracy, respectively, where $p < q$. Assume that the source term in the model advection equation (8) is sufficiently smooth: $\mathcal{F} \in C^{2p}$. Let $u_h \in \mathbb{R}^{n+1}$ be the unique solution to the primal discretzation (9) using D_p. Similarly, let $v_h \in \mathbb{R}^{n+1}$ be the unique solution to the discrete-adjoint problem corresponding to the discrete functional (11) and discretization (9) based on D_p. If $R_{h,q}$ is the discrete residual (13) evaluated using D_q, then the functional error estimate*

$$\delta J_{h,p} \equiv g^T(H_p - H_q)u_h - R_{h,q}(u_h, v_h) \tag{14}$$

is a h^{2p+2}-order accurate approximation to the true functional error, $\delta\mathcal{J}_{h,p} \equiv J_{h,p}(u_h) - \mathcal{J}(\mathcal{U})$.

The proof can be found in Ref. 34. This result indicates that we can recover two additional orders of accuracy in the functional for this particular problem; recall, the superconvergent functional $J_{h,p}(u_h)$ is $\mathrm{O}(h^{2p})$ accurate.

While the above theorem applies only to a very simple example, it is straightforward to extend the result to more general problems and the numerical experiments in Section (IV) demonstrate that it continues to hold for more complex PDEs, such as the Euler equations. In a more general setting, the error estimate has the form

$$\begin{aligned} \delta J_{h,p} &\equiv J_{h,p}(u_h) - J_{h,q}(u_h) - R_{h,q}(u_h, v_h), \\ &= \delta \mathcal{J}_{h,p} + \mathrm{O}(h^{2p-r+3}), \end{aligned} \tag{15}$$

where $r \leq 2$ is the order of the derivative operator present in the continuous PDE and

- u_h is the discrete primal solution based on a discretization using D_p,
- v_h is the discrete adjoint solution based on the primal discretization,
- $J_{h,p}(u_h)$ is the discrete functional with necessary geometric terms approximated using H_p and D_p and evaluated with the state u_h,
- $J_{h,q}(u_h)$ is the discrete functional with necessary geometric terms approximated using H_q and D_q and evaluated with the state u_h, and
- $R_{h,q}(u_h, v_h)$ is the discrete residual based on the operators H_q and D_q and evaluated with the discrete primal and dual states u_h and v_h.

To obtain an error estimate with the predicted asymptotic error, the discrete dual variable v_h must be an $\mathrm{O}(h^{p+1})$ accurate approximation of the continuous dual variable. For example, the discrete dual variable corresponding to the primal problem (9) and functional (11) satisfies the linear equation

$$-\Lambda D_p v_h = -g - H_p^{-1} e_n \, e_n^T \Lambda \left(v_h + \alpha e_n \right). \tag{16}$$

This is an SBP discretization of the continuous dual BVP[b], and v_h has the necessary accuracy to achieve the asymptotically optimal error estimate. More generally, the accuracy requirement on v_h demands that the discretization and discrete functional lead to a consistent and sufficiently accurate discretization of the dual problem. i.e. dual consistency.

Finally, we highlight several interesting characteristics of the functional error estimate (14) relative to other implementations of the adjoint weighted-residual method.

- Finite-element error estimates based on p-enrichment must approximate both the solution and adjoint on the fine space using either patch-based interpolation[35] or smoothing iterations.[15,32] In contrast, the estimate (15) uses the solution u_h and adjoint v_h computed from the discretization based on the SBP operator D_p. In other words, no high order solution or adjoint variable is necessary.
- Finite-volume and finite-difference implementations based on embedded meshes require an explicit interpolation operator.[13,36] The proposed method approximates the residual error using the operator D_q; while D_q defines an implicit reconstruction, no explicit reconstruction is required to implement the method. In addition, refinement-based approaches can lead to large embedded meshes unless the refinement and interpolation are performed on-the-fly:[13] a compromise between memory and coding effort. Here, D_q operates on the same mesh as D_p, so no embedded mesh is necessary when computing the estimate (15). Finally, the proposed error estimate is a factor $\mathrm{O}(h^{3-r})$ more accurate than $J_{h,p}(u_h)$, whereas error estimates based on mesh refinement typically have the same asymptotic convergence rate as the discrete functional, unless Richardson extrapolation is used.[13]

[b]The continuous dual PDE can be found in example 1 of the Appendix.

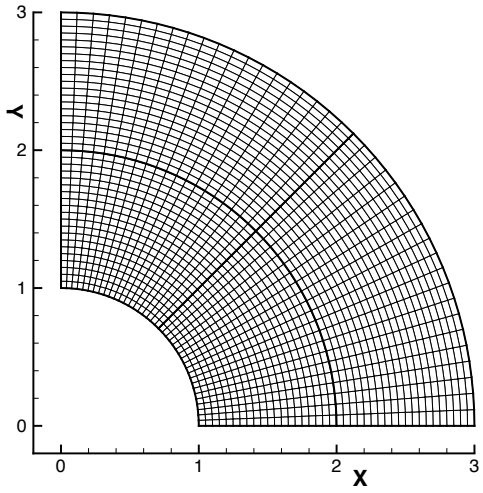

Figure 2. Geometry and block topology for the inviscid-vortex study.

IV. Results

A. Examples of Superconvergence

In this section we verify the theory of SBP-SAT superconvergent functionals. We consider three cases, ranging from a simple flow with an analytical solution to a large-scale 3-dimensional geometry. The results illustrate that, even when theoretical assumptions are violated (e.g., solution smoothness), the benefits of using a dual-consistent discretization are significant.

The dual-consistent and dual-inconsistent schemes used to obtain the following results differ only in the boundary condition and functional implementation. The difference operators, interface SATs, and dissipation operators are identical for both the dual consistent and dual inconsistent schemes. The different implementations amount to the addition of small $\mathrm{O}(h^{p+1})$ corrections to the boundary conditions and functional estimate, where $(p+1)$ is the order of the discrete solution. For specific details on these corrections see Ref. 28.

We emphasize that the results in this section do not require the solution of the adjoint equations: dual consistency or dual inconsistency is implicitly present, and this is sufficient to impact functional accuracy.

1. Vortex Flow

Our first example is a 2-dimensional inviscid vortex whose streamlines are concentric circles about the origin. This isentropic flow has a smooth analytical solution and provides an important verification of the theory. The solution in polar coordinates is defined by

$$\rho(r) = \rho_i \left[1 + \frac{\gamma - 1}{2} M_i^2 \left(1 - \frac{r_i^2}{r^2} \right) \right]^{\frac{1}{\gamma - 1}},$$

with the remaining variables obtained using isentropic relations. The subscript i indicates values along the radius r_i. Here we have chosen $r_i = 1$, $\rho_i = 2$, $M_i = 0.95$, and $p_i = 1/\gamma$, where γ is the ratio of heat capacities.

The geometry and block topology are illustrated in Figure 2. The grid consists of four curvilinear blocks that conform to the domain $\Omega = \{(r, \theta) \mid r \in [1, 3],\, \theta \in [0, \pi/2]\}$. An inviscid-wall boundary condition is applied along the inner radius, $r = 1$, while characteristic boundary conditions supplying the exact solution are applied along the remaining boundaries. For the functional, we calculate a nominal drag defined by the force in the x direction on the curve $\Gamma = \{r = 1, \theta \in [0, \pi/2]\}$. The exact value is given by $D = -1/\gamma$.

To conduct the grid refinement study, an analytical mapping is used to generate a set of 20 grids. Each block on a given grid is discretized uniformly into $(n+1)$ nodes in the radial and angular directions, where

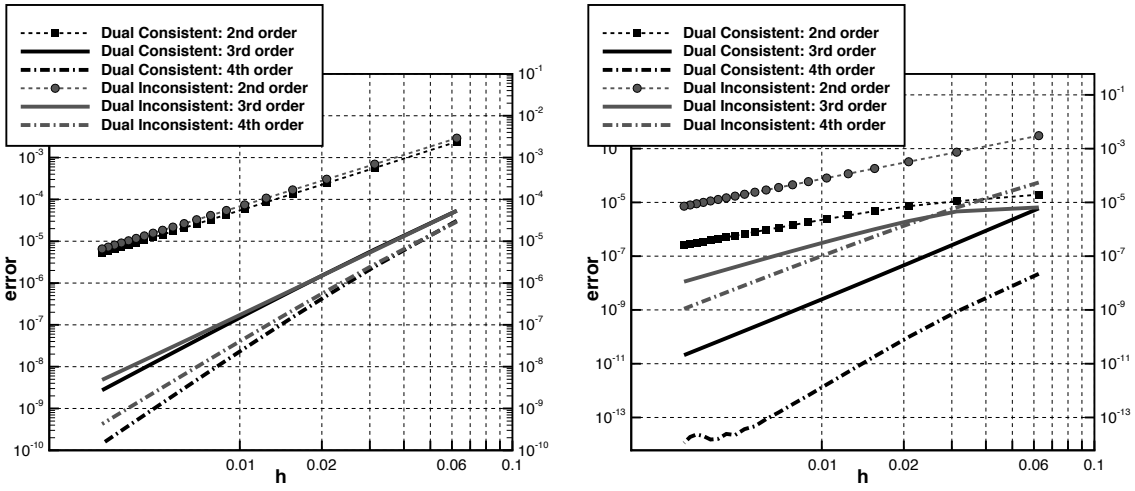

(a) solution error

(b) drag error

Figure 3. Solution errors in the L^2 norm and the drag functional errors for the inviscid vortex flow; note the different y-axis ranges.

Table 1. Functional convergence rate for the inviscid-vortex problem

	solution design accuracy		
	2nd	3rd	4th
dual inconsistent	2.0022	2.9219	3.9397
dual consistent	1.9341	4.0740	5.9095

$n \in \{17 + 16i \mid 0 \leq i \leq 19\}$. Thus, the finest grid consists of 321×321 nodes on each of the four block, or 412 164 nodes in total.

We begin by examining the L^2 error in the solution. Figure 3(a) plots the error in density versus the nominal mesh spacing, $h = 1/n$. Results from second-, third-, and fourth-order accurate SBP operators are included, and both dual-consistent and dual-inconsistent boundary treatments are shown. The figure demonstrates that the discretizations obtain their design order of accuracy. Moreover, dual consistency has little impact on the solution order of accuracy.

Next, we examine the functional error, plotted in Figure 3(b). Here we see a significant difference in error between the dual consistent and dual-inconsistent discretizations. Table 1 lists the order of accuracy of the discrete functional calculated from the results on the finest two grid levels, or the finest two grid levels not affected by round-off errors in the case of the fourth-order dual consistent results. As predicted by the theory, the third- and fourth-order dual-consistent SBP discretizations produce superconvergent functionals.

2. Symmetric Joukowski Airfoil

For our second example, we consider the sectional drag coefficient on a symmetric Joukowski airfoil in a subsonic inviscid flow. For an infinite domain the drag will be zero; however, the finite domain used here has a boundary 10 chord lengths from the airfoil. Imposing the free-stream flow at the finite boundary leads to small errors in the drag coefficient that do not vanish as the grid is refined. Therefore, the grid-converged drag coefficient is not zero.

A set of four C-grids was generated for the grid refinement study. The finest grid consists of 762 032 nodes, with 1556 nodes distributed along the airfoil. The three remaining grid levels are produced by successively removing every other node from the finest grid. The coarsest grid is shown in Figure 4(a), together with a close-up view near the airfoil in Figure 4(b).

No analytical solution is available for the flow around a Joukowski airfoil with a finite boundary, but

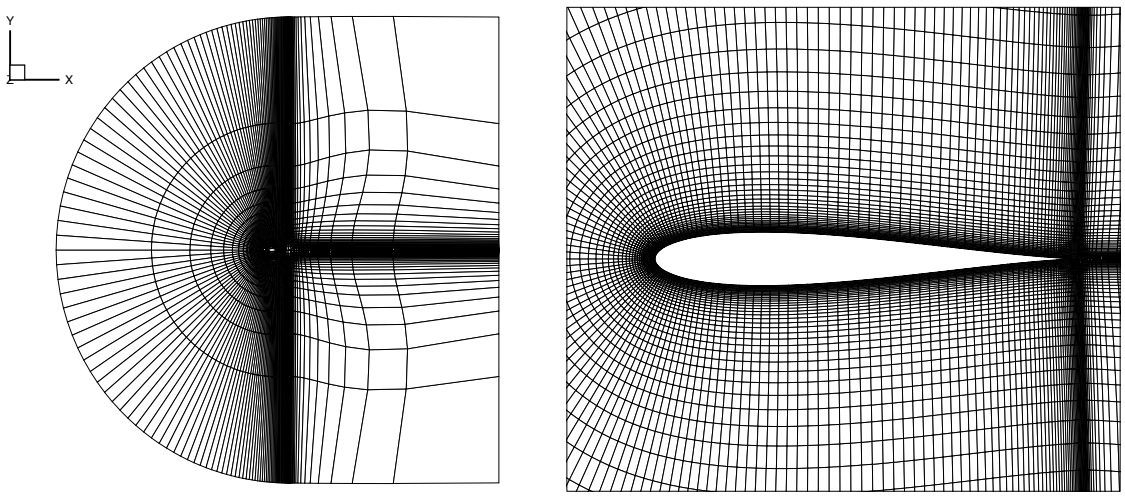

(a) example grid (b) grid close-up

Figure 4. Coarsest grid used in the Joukowski-airfoil study, and a close-up view of the grid near the airfoil

the order of accuracy and limiting value of c_d can be estimated using the methodology of Baker;[37] see also Ref. 38. In brief, a nonlinear equation in the order of accuracy, p, can be constructed using relations between three grid levels — the sequence of functional values must be monotone.

Applying this method to the drag coefficient functional we obtain the values listed in Table 2. The estimated order of accuracy for all the discretizations is lower than predicted by theory, based on the finest sequence of three grids. It is possible that the drag is not yet in the asymptotic regime, or that one of the assumptions of the theory is violated (e.g. the solution is not sufficiently smooth). Nevertheless, it is clear that the third- and fourth-order dual consistent discretizations are converging at a faster rate than their dual inconsistent counterparts.

The limiting value of the drag coefficient estimated from the fourth-order dual consistent discretization, $c_d \approx 2.694127 \times 10^{-6}$, is used in Figure 5 to plot the error versus a normalized mesh spacing. For the third- and fourth-order methods, there is a two order of magnitude improvement going from the dual inconsistent to dual consistent treatment on the three finest grids. Indeed, the third-order dual-consistent functional using the second coarsest grid is more accurate than the third-order dual-inconsistent functional on the finest grid.

3. ONERA M6 Wing

For the final example illustrating the impact of dual consistency on functional accuracy, we consider the ONERA M6 wing at a Mach number of 0.5 and an angle of attack of 3 degrees. In the Joukowski-airfoil study the grid sequence was generated by recursively removing every other node in each coordinate direction. This is the typical approach used for grid convergence studies of one- and two-dimensional problems. In three dimensions, these nested grids increase in size by a factor of 8 between grid levels, and this limits the number of grids that can be included in the sequence.

To overcome the above limitation, we use a multi-block grid consisting of B-spline volumes[39] that define analytical mappings; this permits any integer number of nodes to be used in a given (computational) coordinate direction. Specifically, we consider blocks with 9, 17, 25, 33, and 41 nodes in each direction. The grid consists of 1024 blocks, so the coarsest grid has approximately 7.5×10^5 nodes and the finest has approximately 7.1×10^7 nodes. The use of an analytical mapping ensures that the grids belong to the same family, which is necessary for a rigorous grid refinement study.[2]

Table 3 lists the coefficients of drag computed on each grid using second- and third-order SBP-SAT schemes, with dual inconsistent and dual consistent formulations. In the case of the dual inconsistent third-order method the finest three grids produce a nonmonotone sequence, so we cannot estimate the order of accuracy or limiting value of the functional from these grids.

As with the Joukowski airfoil, the dual consistent schemes converge smoothly with estimated orders that are in reasonable agreement with the design order of accuracy. In contrast, the dual inconsistent schemes

Table 2. Estimated limiting value of c_d as $h \to 0$, and estimated order of accuracy for the symmetric Joukowski airfoil. Nonmonotone sequences or sequences that produce negative p are indicated with a dash. The grids are labeled from from coarsest, 1, to finest, 4.

		dual inconsistent		
		2nd	3rd	4th
Limiting c_d Value	grid set (1,2,3)	7.588×10^{-6}	—	2.662×10^{-6}
	grid set (2,3,4)	2.732×10^{-6}	2.563×10^{-6}	2.676×10^{-6}
Estimated Order	grid set (1,2,3)	0.6640	—	2.6802
	grid set (2,3,4)	1.8666	1.3713	2.7762

		dual consistent		
		2nd	3rd	4th
Limiting c_d Value	grid set (1,2,3)	—	2.697×10^{-6}	2.696×10^{-6}
	grid set (2,3,4)	2.850×10^{-6}	2.694×10^{-6}	2.694×10^{-6}
Estimated Order	grid set (1,2,3)	—	5.4262	6.3234
	grid set (2,3,4)	1.5295	2.3830	4.5682

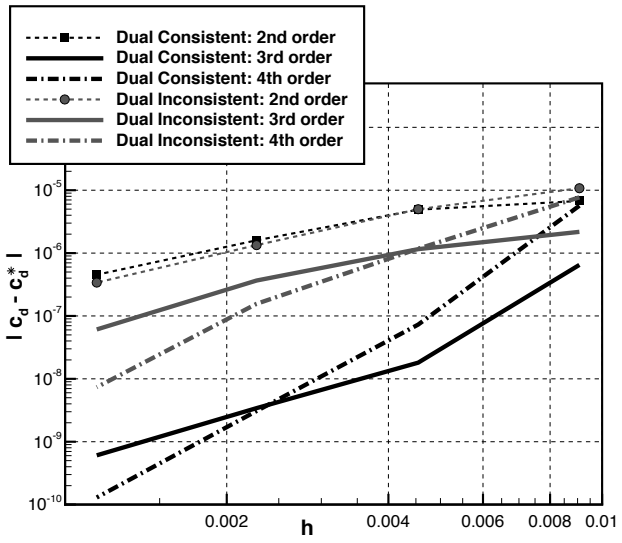

Figure 5. Joukowski study: difference between the drag coefficient and the limiting c_d^* calculated from the fourth-order dual consistent results.

Table 3. Computed drag coefficients for the ONERA M6 wing, together with the estimated limiting value of C_D as $h \to 0$ and the estimated order of accuracy; the latter two are estimated using the 3 finest grids. The order and limiting functional value for the 3rd order dual inconsistent scheme could not be estimated due to a nonmonotone sequence.

	dual inconsistent		dual consistent	
n	2nd	3rd	2nd	3rd
8	4.0397×10^{-3}	4.3826×10^{-3}	4.4100×10^{-3}	4.1071×10^{-3}
16	3.8922×10^{-3}	3.9702×10^{-3}	4.0166×10^{-3}	3.9666×10^{-3}
24	3.9079×10^{-3}	3.9488×10^{-3}	3.9750×10^{-3}	3.9586×10^{-3}
32	3.9203×10^{-3}	3.9467×10^{-3}	3.9647×10^{-3}	3.9576×10^{-3}
40	3.9283×10^{-3}	3.9473×10^{-3}	3.9610×10^{-3}	3.9572×10^{-3}
limiting C_D	3.9846×10^{-3}	—	3.9556×10^{-3}	3.9566×10^{-3}
estimated order	0.7252	—	2.9085	2.8564

converge slowly relative to their design accuracy; the second-order scheme is less than first order and the third-order scheme produces a nonmonotone sequence.

The third-order dual consistent scheme does not appear to be asymptotically superconvergent; nevertheless, this scheme produces the most accurate functional estimates. We postulate that the degraded convergence is the result of nonsmooth features in the flow, e.g. along the trailing-edge and tip vortex. On the second coarsest grid, the estimated percent error in the dual consistent third-order functional is 0.25%. The second-order dual consistent scheme requires a grid approximately 8 times larger to reach this level of accuracy in C_D. The second-order dual inconsistent scheme has not even reached this level using the finest grid, which is approximately 16 times the resolution of the second coarsest grid.

Figure 6 plots the drag coefficient error for the four schemes considered. The error is approximated using the limiting value of the drag coefficient predicted by the third-order dual consistent scheme. The nominal mesh spacing is defined by $h = 8/n$, where n is the number of intervals in each direction on the blocks. The well-behaved convergence of the dual consistent schemes is clearly visible in the figure. The third-order estimates initially converge at the theoretically predicted fourth-order rate before reducing to third order. As mentioned above, this may be caused by the trailing edge or tip vortex, which violate the smoothness assumptions required by the theory. Asymptotically, the dual inconsistent schemes produce relatively large errors. The second-order scheme appears to yield a first-order C_D error, consistent with the estimated order in Table 3. The third-order scheme exhibits rapid convergence for large h followed by slow convergence for small h. Indeed, there appears to be a singularity of the type described by Salas and Atkins near $h = 0.4$ in the dual inconsistent third-order results.

B. Error Estimation Examples

The next set of results illustrate the impact of dual consistency on error estimates. Here, the adjoint solution must be computed explicitly, unlike the previous section. We use GCROT(m, k),[40] a variant of the truncated GCRO iterative solver,[41,42] to solve the adjoint linear system. The adjoint linear system involves the transpose of the flow Jacobian matrix; however, GCROT(m, k), like all Krylov solvers based on Arnoldi's method, requires only products of the transposed Jacobian with arbitrary vectors. The necessary matrix-vector products are evaluated using a hand-coded version of reverse-mode algorithmic differentiation.[43–45] The adjoint system is preconditioned using a transposed variant of the parallel approximate-Schur preconditioner[46] used in the primal solution algorithm.

Both the primal and dual problems are solved to machine tolerance to avoid confounding effects introduced by partially converged iterative solutions; however, in practice, the tolerances should be adjusted dynamically to avoid oversolving the systems when the functional error is large.

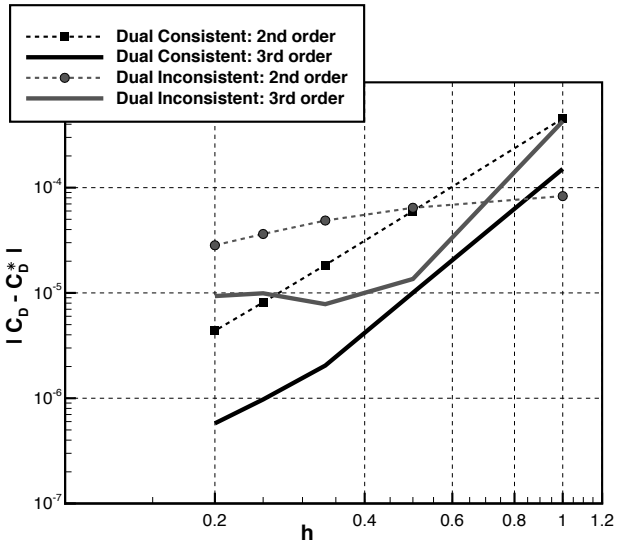

Figure 6. ONERA M6 study: difference between the C_D functional and the limiting C_D^* from the third-order dual consistent scheme.

1. Vortex Flow

As a simple verification of SBP error-estimate theory, we return to the inviscid vortex flow described in Section IV.A.1. The functional remains the force in the x-direction along the inner radius, and the error estimation procedure is applied on the same sequence of 20 grids.

Figure 7(a) plots the error-estimation results using a second-order discretization ($p = 1$) and fourth-order residual reconstruction ($q = 2$). Both the dual-consistent and dual-inconsistent schemes yield second-order accurate functionals. The error estimates from the two schemes are also second-order, but the dual consistent error estimate is significantly more accurate. Indeed, the dual consistent corrected functional is fourth-order accurate, as predicted by the theory. The dual-inconsistent corrected functional is three times more accurate than the baseline functional, but is only second-order accurate.

The error-estimation results for $p = 2$ and $q = 3$ are even more striking; see Figure 7(b). The dual-inconsistent error estimate significantly under predicts the error for most of the grids considered; consequently, the dual-inconsistent baseline functional and corrected functional are not significantly different in terms of accuracy. Contrast this behaviour with the dual-consistent results: not only is the dual-consistent baseline functional superconvergent, its corresponding error estimate produces an asymptotically sixth-order corrected functional. On the finest grid the two error estimates are separated by six-orders of magnitude, a substantial difference considering the two flow solutions are nominally the same order of accuracy.

2. NACA0012 Airfoil

For a more practical example of SBP error estimation, we consider the drag on an airfoil in subsonic flow. We adopt the modified NACA0012 airfoil and grid described in Ref. 1. Briefly, the NACA0012 airfoil is modified to have a sharp trailing edge and an O-grid is generated around the airfoil using a Karman-Trefftz conformal mapping. The grid is partitioned into 256 blocks of equal dimension, $(n + 1) \times (n + 1)$. For the coordinate dimensions we consider $n \in \{16, 32, 64, 128, 256\}$. The largest grid with $n = 256$ is used only to obtain an estimate of the asymptotic drag value, as described below

The free-stream Mach number is $M = 0.5$ and the angle of attack is 1.25 degrees. These conditions define a free-stream state that is imposed at the far-field boundary using characteristic-based SAT penalties. The far-field boundary is approximately 150 chord lengths from the airfoil. No circulation correction is applied at the far-field.

The NACA0012 boundary-value problem considered here has no known analytical solution; hence, to calculate errors in the drag we must rely on a sufficiently accurate approximation of the drag functional. As with the Joukowski and ONERA M6 cases, we use a Richardson extrapolation following the methodology of

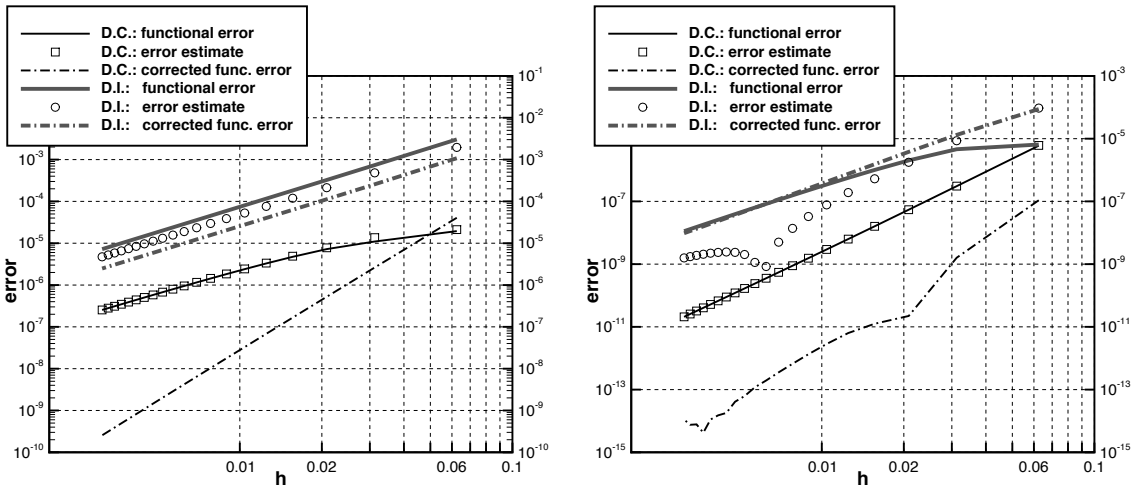

(a) $(p, q) = (1, 2)$ (b) $(p, q) = (2, 3)$

Figure 7. Results for the vortex flow functional error estimation.

Baker.[37] The extrapolation is based on the drag values from the third-order dual-consistent scheme on the three finest grids (including $n = 256$).

Figure 8(a) plots the drag error, estimated error, and corrected-drag error for the second-order discretization and fourth-order residual reconstruction. The dual-consistent and dual-inconsistent schemes produce drag values with comparable errors; however, the dual-consistent error estimate is more accurate than the dual-inconsistent error estimate, which under predicts the baseline-drag error. The dual-consistent error estimate leads to a corrected drag that is $\mathrm{O}(h^{2.5})$ asymptotically and an order of magnitude more accurate than the corresponding dual-inconsistent value on the finest grid.

Results for the third-order discretization are plotted in Figure 8(b). Here, the dual-consistent error estimate systematically under predicts the baseline-drag error. Nevertheless, the corrected-drag error is approximately three times smaller than the baseline-drag error, although both have similar asymptotic behaviour. In contrast, the dual-inconsistent error estimate significantly over predicts the drag error, leading to a corrected drag that is less accurate than the baseline drag.

The baseline drag of the third-order dual-inconsistent scheme is remarkably accurate; however, we believe that this anomalous behaviour is caused by an error cancellation of the type studied in Ref. 2. For some mesh size $h \in [0.02, 0.03]$, the signed errors present in the functional cancel perfectly. In other words, the dual-inconsistent scheme "got lucky" here. This type of cancellation cannot be relied upon to reduce the error on a given mesh. Indeed, it is this type of cancellation that can increase the error during refinement.

The reduced accuracy of the error estimates in the present example can be traced to the nonsmoothness of the primal and adjoint solutions. The primal flow solution is nonsmooth at the finite-angle trailing edge: to first order the velocity field behaves as $r^{\delta/(2\pi-\delta)}$, where r is the radial distance from the trailing edge and δ is the included angle of the trailing edge. In addition, the adjoint variable corresponding to ρv has a singularity at the trailing edge. These properties of the analytical primal and adjoint solutions limit the asymptotic convergence rate of u_h and v_h, and, consequently, the convergence rate of the discrete functional and error estimate. Nevertheless, despite a degraded asymptotic convergence rate, the results in Figure 8 clearly demonstrate that the dual consistent schemes produce much more accurate error estimates than the dual inconsistent schemes.

V. Conclusion

A dual consistent discretization is one that leads to a set of discrete adjoint equations that converge to the continuous adjoint equations. We have shown that a dual consistent discretization of the Euler equations using an SBP-SAT finite-difference discretization can significantly improve the accuracy of functional estimates. Moreover, the results suggest that dual consistency may resolve functional convergence issues of the

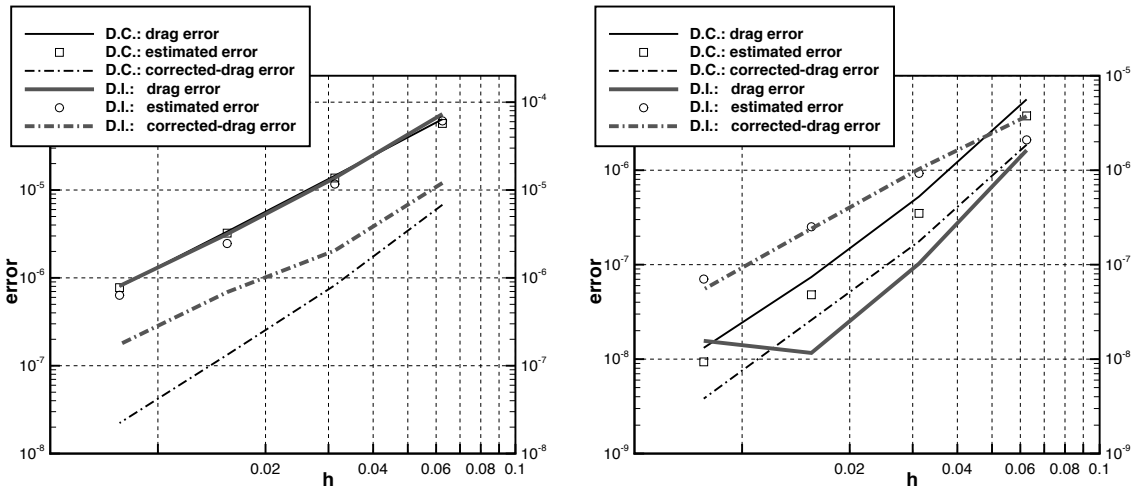

(a) $(p, q) = (1, 2)$ (b) $(p, q) = (2, 3)$

Figure 8. Results for the NACA0012 drag error estimation.

type described by Salas and Atkins.[2] Finally, we have also demonstrated that a dual-consistent formulation leads to improved error estimates from the adjoint-weighted residual method.

The importance of dual consistency for functional accuracy in Galerkin finite-element methods is well known. However, the results presented here suggest that dual consistency, like the consistency and stability of the primal equations, is a property of fundamental importance to all forms of discretization. As we have shown, a high-order, yet dual inconsistent, SBP-SAT discretization may not predict functionals with sufficient accuracy to outperform a second-order scheme in terms of efficiency. In contrast, high-order dual consistent discretizations are often orders of magnitude more accurate than a second-order scheme on the same grid.

Dual consistency is a property of the discrete primal equations and the discrete functional, so a scheme does not need to solve the adjoint equations explicitly to enjoy the potential benefits[c]. Unfortunately, constructing a high-order dual consistent scheme may not be straightforward in all cases. For example, it is not clear how dual consistent boundary conditions might be constructed for a high-order cell-centered finite-volume method.

Acknowledgments

The authors gratefully acknowledge financial assistance from Bombardier Aerospace, the Natural Sciences and Engineering Research Council (NSERC), the Canada Research Chairs program, Mathematics of Information Technology and Complex systems (MITACS), and the University of Toronto.

Computations were performed on the general purpose cluster at the SciNet HPC Consortium. SciNet is funded by: the Canada Foundation for Innovation under the auspices of Compute Canada; the Government of Ontario; Ontario Research Fund - Research Excellence; and the University of Toronto.

A. Example dual problems

Example 1: Consider the first-order BVP

$$\begin{aligned} \frac{d}{dx}\left(\lambda \mathcal{U}\right) - \mathcal{F} &= 0, \qquad \forall\, x \in [0,1] \\ \mathcal{U}(0) &= \alpha, \end{aligned} \tag{17}$$

[c]Of course, the adjoint variables are required for error estimates based on the adjoint-weighted residual method.

and the linear functional

$$\mathcal{J} = \int_0^1 \mathcal{G}\mathcal{U}\, dx + \rho\mathcal{U}(1). \tag{18}$$

The inner product of (17) with an arbitrary $\mathcal{V} \in L^2[0,1]$ yields zero. Thus, subtracting this inner product from $\mathcal{J}$ does not change the functional's value and applying integration by parts, we find

$$\begin{aligned}\mathcal{J} &= \int_0^1 \mathcal{G}\mathcal{U}\, dx + \rho\mathcal{U}(1) - \underbrace{\int_0^1 \mathcal{V}\left[\frac{d}{dx}(\lambda\mathcal{U}) - \mathcal{F}\right] dx}_{(\mathcal{V}, L\mathcal{U}-\mathcal{F})_\Omega} \\ &= \int_0^1 \mathcal{V}\mathcal{F}\, dx + \alpha\lambda\mathcal{V}(0) - \underbrace{\int_0^1 \mathcal{U}\left[-\lambda\frac{d}{dx}(\mathcal{V}) - \mathcal{G}\right] dx}_{(L^*\mathcal{V}-\mathcal{G}, \mathcal{U})_\Omega} + \underbrace{\mathcal{U}(1)\left[\rho - \lambda\mathcal{V}(1)\right]}_{-\mathcal{B}_{\partial\Omega}(\mathcal{U},\mathcal{V})}.\end{aligned}$$

The terms under the braces relate this particular example with the general case described in Section II.A. The above expression is true for any $\mathcal{V} \in L^2[0,1]$. However, if $\mathcal{V}$ satisfies the dual problem

$$\begin{aligned} -\lambda\frac{d}{dx}(\mathcal{V}) - \mathcal{G} = 0, \qquad \forall\, x \in [0,1] \\ \lambda\mathcal{V}(1) = \rho, \end{aligned} \tag{19}$$

then the functional simplifies and becomes independent of $\mathcal{U}$:

$$\mathcal{J} = \int_0^1 \mathcal{V}\mathcal{F}\, dx + \alpha\lambda\mathcal{V}. \tag{20}$$

Thus, the primal problem defined by (17) and (18) can be reformulated into the dual (adjoint) problem defined by (19) and (20). In this example, the primal and adjoint differential operators are given by $\frac{d}{dx}(\lambda)$ and $-\lambda\frac{d}{dx}$, respectively.

Example 2: Consider the second-order BVP

$$\frac{d}{dx}\left(\gamma\frac{d\mathcal{U}}{dx}\right) - \mathcal{F} = 0, \qquad \forall\, x \in [0,1], \tag{21}$$

$$\mathcal{U}(0) = \alpha, \qquad \frac{d\mathcal{U}}{dx}(1) = \beta, \tag{22}$$

and the linear functional

$$\mathcal{J} = \int_0^1 \mathcal{G}\mathcal{U}\, dx + \rho\mathcal{U}(1) + \sigma\frac{d\mathcal{U}}{dx}(0).$$

Taking the integral inner product of (21) with $\mathcal{V} \in L^2[0,1]$ and subtracting this null term from $\mathcal{J}$ and rearranging, we find

$$\begin{aligned}\mathcal{J} &= \int_0^1 \mathcal{G}\mathcal{U}\, dx + \rho\mathcal{U}(1) + \sigma\frac{d\mathcal{U}}{dx}(0) - \underbrace{\int_0^1 \mathcal{V}\left[\frac{d}{dx}\left(\gamma\frac{d\mathcal{U}}{dx}\right) - \mathcal{F}\right] dx}_{(\mathcal{V}, L\mathcal{U}-\mathcal{F})_\Omega} \\ &= \int_0^1 \mathcal{V}\mathcal{F}\, dx - \gamma\beta\mathcal{V}(1) - \gamma\alpha\frac{d\mathcal{V}}{dx}(0) \\ &\quad - \underbrace{\int_0^1 \mathcal{U}\left[\frac{d}{dx}\left(\gamma\frac{d\mathcal{V}}{dx}\right) - \mathcal{G}\right] dx}_{(L^*\mathcal{V}-\mathcal{G}, \mathcal{U})_\Omega} + \underbrace{\mathcal{U}(1)\left[\gamma\frac{d\mathcal{V}}{dx}(1) + \rho\right] + \frac{d\mathcal{U}}{dx}(0)\left[\gamma\mathcal{V}(0) + \sigma\right]}_{-\mathcal{B}_{\partial\Omega}(\mathcal{U},\mathcal{V})}.\end{aligned}$$

The functional will be independent of $\mathcal{U}$ if the terms in the second line above vanish. This yields the following adjoint BVP that $\mathcal{V}$ must satisfy.

$$\frac{d}{dx}\left(\gamma\frac{d\mathcal{V}}{dx}\right) - \mathcal{G} = 0, \qquad \forall\, x \in [0,1]$$

$$\gamma\mathcal{V}(0) = -\sigma, \qquad \gamma\frac{d\mathcal{V}}{dx}(1) = -\rho.$$

If $\mathcal{V}$ satisfies the above adjoint problem, then the dual formulation of the functional becomes

$$\mathcal{J} = \int_0^1 \mathcal{V}\mathcal{F}\,dx - \gamma\beta\mathcal{V}(1) - \gamma\alpha\frac{d\mathcal{V}}{dx}(0).$$

Notice that, in contrast with the previous (hyperbolic) example, the differential operator is the same for both the primal and dual problems, i.e. the operator is self-adjoint.

References

[1]Vassberg, J. C. and Jameson, A., "In pursuit of grid convergence for two-dimensional Euler solutions," *AIAA Journal*, Vol. 47, No. 4, July–August 2010.

[2]Salas, M. D. and Atkins, H. L., "On problems associated with grid convergence of functionals," *Computers and Fluids*, Vol. 38, No. 7, 2009, pp. 1445–1454.

[3]Pironneau, O., "On optimum design in fluid mechanics," *Journal of Fluid Mechanics*, Vol. 64, No. 1, 1974, pp. 97–110.

[4]Jameson, A., "Aerodynamic design via control theory," *Journal of Scientific Computing*, Vol. 3, No. 3, 1988, pp. 233–260.

[5]Jameson, A. and Reuther, J., "Control theory based airfoil design using Euler equations," *AIAA/USAF/NASA/ISSMO Symposium on Multidisciplinary Analysis and Optimization*, Panama City Beach, Sept. 1994.

[6]Reuther, J. J., Jameson, A., Alonso, J. J., Rimlinger, M. J., and Saunders, D., "Constrained multipoint aerodynamic shape optimization using an adjoint formulation and parallel computers, part 1," *AIAA Journal*, Vol. 36, No. 1, Jan. 1999, pp. 51–60.

[7]Reuther, J. J., Jameson, A., Alonso, J. J., Rimlinger, M. J., and Saunders, D., "Constrained multipoint aerodynamic shape optimization using an adjoint formulation and parallel computers, part 2," *AIAA Journal*, Vol. 36, No. 1, Jan. 1999, pp. 61–74.

[8]Anderson, W. K. and Bonhaus, D. L., "Airfoil design on unstructured grids for turbulent flows," *AIAA Journal*, Vol. 37, No. 2, Feb. 1999, pp. 185–191.

[9]Driver, J. and Zingg, D. W., "Numerical aerodynamic optimization incorporating laminar-turbulent transition prediction," *AIAA Journal*, Vol. 45, No. 8, Aug. 2007, pp. 1810–1818.

[10]Becker, R., Johnson, C., and Rannacher, R., "Adaptive error control for multigrid finite element methods," Vol. 55, No. 4, 2000, pp. 271–288.

[11]Pierce, N. A. and Giles, M. B., "Adjoint recovery of superconvergent functionals from PDE approximations," *SIAM Review*, Vol. 42, No. 2, 2000, pp. 247–264.

[12]Giles, M. B. and Süli, E., "Adjoint methods for PDEs: a posteriori error analysis and postprocessing by duality," *Acta Numerica*, Vol. 11, 2002, pp. 145–236.

[13]Venditti, D. A. and Darmofal, D. L., "Adjoint error estimation and grid adaptation for functional outputs: application to quasi-one-dimensional flow," *Journal of Computational Physics*, Vol. 164, No. 1, 2000, pp. 204–227.

[14]Nemec, M., Aftosmis, M. J., and Wintzer, M., "Adjoint-based adaptive mesh refinement for complex geometries," *The 46th AIAA Aerospace Sciences Meeting and Exhibit*, No. AIAA–2008–725, Reno, Nevada, United States, Jan. 2008.

[15]Fidkowski, K. J. and Roe, P. L., "An entropy adjoint approach to mesh refinement," *SIAM Journal on Scientific Computing*, Vol. 32, No. 3, 2010, pp. 1261–1287.

[16]Baysal, O. and Eleshaky, M. E., "Aerodynamic sensitivity analysis methods for the compressible Euler equations," *Journal of Fluids Engineering*, Vol. 113, No. 4, 1991, pp. 681–688.

[17]Frank, P. D. and Shubin, G. R., "A comparison of optimization-based approaches for a model computational aerodynamics design problem," *Journal of Computational Physics*, Vol. 98, No. 1, Jan. 1992, pp. 74–89.

[18]Griewank, A., *Evaluating Derivatives*, SIAM, Philadelphia, PA, 2000.

[19]Squire, W. and Trapp, G., "Using complex variables to estimate derivatives of real functions," *SIAM Review*, Vol. 40, No. 1, 1998, pp. 110–112.

[20]Martins, J. R. R. A., Sturdza, P., and Alonso, J. J., "The complex-step derivative approximation," *ACM Transactions on Mathematical Software*, Vol. 29, No. 3, Sept. 2003, pp. 245–262.

[21]Collis, S. S. and Heinkenschloss, M., "Analysis of the streamline upwind/Petrov Galerkin method applied to the solution of optimal control problems," Tech. Rep. TR02-01, Houston, Texax, 2002.

[22]Lu, J. C.-C., *An a posteriori error control framework for adaptive precision optimization using discontinuous Galerkin finite element method*, Ph.D. thesis, Massachusetts Institute of Technology, Cambridge, Massachusetts, 2005.

[23]Hartmann, R., "Error estimation and adjoint based refinement for an adjoint consistent DG discretization of the compressible Euler equations," *International Journal of Computing Science and Mathematics*, Vol. 1, No. 2–4, pp. 207–220.

[24]Lanczos, C., *Linear Differential Operators*, D. Van Nostrand Company, Limited, London, England, 1961.

[25]Pierce, N. A. and Giles, M. B., "An introduction to the adjoint approach to design," *Flow, Turbulence and Combustion*, Vol. 65, No. 3, 2000, pp. 393–415.

[26]Kreiss, H.-O. and Scherer, G., "Finite element and finite difference methods for hyperbolic partial differential equations," *Mathematical Aspects of Finite Elements in Partial Differential Equations*, edited by C. de Boor, Mathematics Research Center, the University of Wisconsin, Academic Press, 1974.

[27]Svärd, M., "On coordinate transformations for summation-by-parts operators," *Journal of Scientific Computing*, Vol. 20, No. 1, Feb. 2004, pp. 29–42.

[28]Hicken, J. E. and Zingg, D. W., "Superconvergent functional estimates from summation-by-parts finite-difference discretizations," *SIAM Journal on Scientific Computing*, Vol. 33, No. 2, 2011, pp. 893–922.

[29]Funaro, D. and Gottlieb, D., "A new method of imposing boundary conditions in pseudospectral approximations of hyperbolic equations," *Mathematics of Computation*, Vol. 51, No. 184, Oct. 1988, pp. 599–613.

[30]Carpenter, M. H., Gottlieb, D., and Abarbanel, S., "Time-stable boundary conditions for finite-difference schemes solving hyperbolic systems: methodology and application to high-order compact schemes," *Journal of Computational Physics*, Vol. 111, No. 2, 1994, pp. 220–236.

[31]Gustafsson, B., "The convergence rate for difference approximations to general mixed initial boundary value problems," *SIAM Journal on Numerical Analysis*, Vol. 18, No. 2, April 1981.

[32]Fidkowski, K. J. and Darmofal, D. L., "Review of output-based error estimation and mesh adaptation in computational fluid dynamics," *AIAA Journal*, Vol. 49, No. 4, 2011, pp. 673–694.

[33]Hicken, J. E. and Zingg, D. W., "Summation-by-parts operators and high-order quadrature," *Applied Numerical Mathematics*, submitted Mar 2011, pp. 18.

[34]Hicken, J. E., "Output error estimation for summation-by-parts finite-difference schemes," *Journal of Computational Physics*, submitted June 2011, pp. 25.

[35]Rannacher, R., "Adaptive Galerkin finite element methods for partial differential equations," *Journal of Computational and Applied Mathematics*, Vol. 128, No. 1–2, 2001, pp. 205–233.

[36]Nemec, M. and Aftosmis, M. J., "Adjoint error estimation and adaptive refinement for embedded-boundary Cartesian meshes," *18th AIAA Computational Fluid Dynamics Conference*, No. AIAA–2007–4187, Miami, Florida, United States, June 2007.

[37]Baker, T. J., "Mesh generation: Art or science?" *Progress in Aerospace Sciences*, Vol. 41, No. 1, 2005, pp. 29–63.

[38]Vassberg, J. C. and Jameson, A., "In pursuit of grid convergence, part 1: two-dimensional Euler solutions," *27th AIAA Applied Aerodynamics Conference*, No. AIAA–2009–4114, San Antonio, Texas, 2009.

[39]Hicken, J. E. and Zingg, D. W., "Aerodynamic optimization algorithm with integrated geometry parameterization and mesh movement," *AIAA Journal*, Vol. 48, No. 2, Feb. 2010, pp. 400–413.

[40]Hicken, J. E. and Zingg, D. W., "A simplified and flexible variant of GCROT for solving nonsymmetric linear systems," *SIAM Journal on Scientific Computing*, Vol. 32, No. 3, 2010, pp. 1672–1694.

[41]de Sturler, E., "Nested Krylov methods based on GCR," *Journal of Computational and Applied Mathematics*, Vol. 67, 1996, pp. 15–41.

[42]de Sturler, E., "Truncation strategies for optimal Krylov subspace methods," *SIAM Journal on Numerical Analysis*, Vol. 36, No. 3, 1999, pp. 864–889.

[43]Barth, T. J. and Linton, S. W., "An unstructured mesh Newton solver for compressible fluid flow and its parallel implementation," *33rd AIAA Aerospace Sciences Meeting and Exhibit*, No. AIAA–95–0221, Reno, Nevada, 1995.

[44]Anderson, W. K. and Bonhaus, D. L., "Airfoil design on unstructured grids for turbulent flows," *AIAA Journal*, Vol. 37, No. 2, Feb. 1999, pp. 185–191.

[45]Giles, M. B., Duta, M. C., Müller, J.-D., and Pierce, N. A., "Algorithm developments for discrete adjoint methods," *AIAA Journal*, Vol. 41, No. 2, Feb. 2003, pp. 198–205.

[46]Saad, Y. and Sosonkina, M., "Distributed Schur complement techniques for general sparse linear systems," *SIAM Journal of Scientific Computing*, Vol. 21, No. 4, 1999, pp. 1337–1357.